⌘ *Author's Choice*

THE JOURNAL OF BIOLOGICAL CHEMISTRY VOL. 286, NO. 5, pp. 3315–3322, February 4, 2011


# Molecular Characterization of a Novel Geranylgeranyl Pyrophosphate Synthase from *Plasmodium* Parasites*[S]

Received for publication, June 11, 2009, and in revised form, November 3, 2010 Published, JBC Papers in Press, November 17, 2010, DOI 10.1074/jbc.M109.027235

**Jennifer D. Artz[‡], Amy K. Wernimont[‡], James E. Dunford[§¶], Matthieu Schapira[‡‖], Aiping Dong[‡], Yong Zhao[‡], Jocelyne Lew[‡], R. Graham G. Russell[¶], F. Hal Ebetino[**], Udo Oppermann[§¶], and Raymond Hui[‡1]**

*From the [‡]Structural Genomics Consortium, University of Toronto, Toronto, Ontario M5G 1L7, Canada, the [§]Structural Genomics Consortium, University of Oxford, Old Road Campus Research Building, Oxford OX3 7DQ, United Kingdom, the [¶]Botnar Research Centre, Oxford Biomedical Research Unit, Oxford OX3 7LD, United Kingdom, the [‖]Department of Pharmacology and Toxicology, University of Toronto, Toronto, Ontario M5S 1A8, Canada, and [**]Procter and Gamble Pharmaceuticals, Inc., Mason, Ohio 45040*

**We present here a study of a eukaryotic *trans*-prenylsynthase from the malaria pathogen *Plasmodium vivax*. Based on the results of biochemical assays and contrary to previous indications, this enzyme catalyzes the production of geranylgeranyl pyrophosphate (GGPP) rather than farnesyl pyrophosphate (FPP). Structural analysis shows that the product length is constrained by a hydrophobic cavity formed primarily by a set of residues from the same subunit as the product as well as at least one other from the dimeric partner. Furthermore, *Plasmodium* GGPP synthase (GGPPS) can bind nitrogen-containing bisphosphonates (N-BPs) strongly with the energetically favorable cooperation of three $Mg^{2+}$, resulting in inhibition by this class of compounds at $IC_{50}$ concentrations below 100 nM. In contrast, human and yeast GGPPSs do not accommodate a third magnesium atom in the same manner, resulting in their insusceptibility to N-BPs. This differentiation is in part attributable to a deviation in a conserved motif known as the second aspartate-rich motif: whereas the aspartates at the start and end of the five-residue motif in FFPP synthases and *P. vivax* GGPPSs both participate in the coordination of the third $Mg^{2+}$, an asparagine is featured as the last residue in human and yeast GGPPSs, resulting in a different manner of interaction with nitrogen-containing ligands.**

Isoprenoids make up the largest family of natural products and drugs derived from the five-carbon isoprene subunit. As precursors to steroids and sterols, they are utilized by prokaryotes and eukaryotes alike to modify proteins, such as G proteins, kinases, and phosphatases, and facilitate their localization to membranes. The production of isoprenoids begins with the synthesis of isopentenyl pyrophosphate (IPP)[2] and dimethylallyl pyrophosphate (DMAPP) via either the mevalonate or nonmevalonate pathway. In most organisms, the first functionally significant product is farnesyl pyrophosphate (FPP). Condensation of FPP with another IPP molecule generates geranylgeranyl pyrophosphate (GGPP), which in turn begets successively longer isoprenoids as products of similar reactions constituting a multistep biopolymerization process. Chemists have designed numerous pyrophosphate analogs, including bisphosphonates, which feature substitution of oxygen by carbon as a phosphate linker. Nitrogen-containing bisphosphonates (N-BPs) have specifically been developed for bone diseases, targeting farnesyl pyrophosphate synthase (FPPS) (1–3), the producer of FPP with low nanomolar $IC_{50}$ values in biochemical assays (3). These compounds are generally less effective against human and *Saccharomyces cerevisiae* geranylgeranyl pyrophosphate synthase (GGPPS), with high nanomolar or low micromolar $IC_{50}$ values (4–6). On the other hand, alkylbisphosphonates (A-BPs) are capable of inhibiting the ability of GGPPS to convert FPP to GGPP at mid-nanomolar $IC_{50}$ values (6). Crystallographic structures of human FPPS as well as human and yeast GGPPS, including complexes with products, substrates, and/or various inhibitors bound have led to descriptions of mechanisms of enzymatic action and inhibition (3, 6–8). One noteworthy observation is the number of magnesium atoms found to coordinate N-BPs in these structures, consistently three in FPPS and two in GGPPS (6).

Because isoprenoids are universally essential, bisphosphonates with and without nitrogen have also been tested as po-

* This work was supported by the Canadian Institutes for Health Research, the Canadian Foundation for Innovation, Genome Canada through the Ontario Genomics Institute, GlaxoSmithKline, the Knut and Alice Wallenberg Foundation, the Ontario Innovation Trust, the Ontario Ministry for Research and Innovation, Merck & Co., Inc., the Novartis Research Foundation, the Petrus and Augusta Hedlund's Foundation, the Swedish Agency for Innovation Systems, the Swedish Foundation for Strategic Research, and the Wellcome Trust (all to the Structural Genomics Consortium, registered charity number 1097737).

⌘ *Author's Choice*—Final version full access.

[S] The on-line version of this article (available at http://www.jbc.org) contains supplemental Figs. S1–S3.

*The atomic coordinates and structure factors (codes 3MAV, 3PH7, and 3LDW) have been deposited in the Protein Data Bank, Research Collaboratory for Structural Bioinformatics, Rutgers University, New Brunswick, NJ (http://www.rcsb.org/).*

[1] To whom correspondence should be addressed: Structural Genomics Consortium, University of Toronto, 101 College St., MaRS South Tower, Toronto, ON M5G 1L7, Canada. Tel.: 416-946-7182; Fax: 416-946-0588; E-mail: raymond.hui@utoronto.ca.

[2] The abbreviations used are: IPP, isopentenyl pyrophosphate; A-BP, alkylbisphosphonate; CLD, chain length-determining; CpNPPPS, *Cryptosporidium parvum* nonspecific polyprenyl pyrophosphate synthase; DMAPP, dimethylallyl pyrophosphate; FARM, first aspartate-rich motif; FPP, farnesyl pyrophosphate; FPPS, farnesyl pyrophosphate synthase; GGPP, geranylgeranyl pyrophosphate; GGPPS, geranylgeranyl pyrophosphate synthase; HsFPPS, human FPPS; HsGGPPS, human GGPPS; IBAN, ibandronate; N-BP, nitrogen-containing bisphosphonate; PDB, Protein Data Bank; PvGGPPS, *Plasmodium vivax* GGPPS; RIS, risedronte; SARM, second aspartate-rich motif; ScGGPPS, *Saccharomyces cerevisiae* GGPPS; TCEP, 1,2,3-tris(2-cyanoethoxy)propane; ZOL, zoledronate.

tential drugs against protozoan pathogens. Infection by trypanosomatids can be arrested by N-BPs at $IC_{50}$ concentrations from low micromolar to nanomolar (9–11). In contrast, apicomplexan parasites have shown nonuniform susceptibility. For example, risedronate (RIS) and zoledronate (ZOL) can both be effective in impairing development of *Toxoplasma gondii*, *Cryptosporidium parvum* and *Eimeria histolytica* (10, 12), whereas *Plasmodium falciparum* cultures are less sensitive to N-BPs in the tests reported to date but can be controlled effectively by a number of A-BPs (4, 10, 13, 14). Recently, lipophilic bisphosphonates have been found to be effective in inhibiting liver stage infection in a mouse model (15).

Biochemical and structural studies on some of the protozoan enzymatic targets of bisphosphonates are also available to corroborate the parasitic disease models. For example, *Trypanosoma cruzi* FPPS is susceptible to nanomolar inhibition by RIS, with the mechanism elucidated by structural evidence (11). The *T. gondii* FPPS, also sensitive to inhibition by N-BPs, produces FPP along with a low level of GGPP when dosed with a high concentration of FPP (16); however, this bifunctional behavior is upstaged by a *C. parvum* nonspecific polyprenyl pyrophosphate synthase (CpNPPPS) that can synthesize a great range of products from C20 to C40 and can be inhibited by N-BPs at $IC_{50}$ concentrations below 100 nM (12). Structural analysis identified the deviation in the chain length-determining (CLD) region of the *Cryptosporidium* enzyme critical in accommodating large products.

According to the PlasmoDB data base (17), there is only one *Plasmodium* enzyme homologous in sequence to human FPPS and GGPPS. The *Plasmodium vivax* ortholog can be inhibited by N-BPs and A-BPs (15, 18). Here, we present the findings of an investigation of the same *P. vivax* protein, focusing on enzymatic function and using crystallography to explain the mechanism of inhibition by bisphosphonates.

## EXPERIMENTAL PROCEDURES

*Reagents*—All inhibitors used in this study, namely RIS, ZOL, and ibandronate (IBAN) were provided by Procter & Gamble Pharmaceuticals (Cincinnati, OH). The *P. vivax* Salvador I cDNA was a generous gift from Prof. Liwang Cui of Penn State University.

*Cloning, Expression, and Purification of Plasmodium PVX_092040*—Full-length *P. vivax* protein encoded by PVX_092040 (17) with an N-terminal $His_6$ tag and TEV cleavage site (MGSSHHHHHHSSGRENLYFQ*G) was cloned from a *P. vivax* Salvador I cDNA library, expressed, and purified according to protocols described previously (19).

*Enzymatic Characterization of PvGGPPS: Activity, Inhibition, and Product Studies*—The activity of PvGGPPS[3] was measured by a $^{14}C$ radioactivity assay using the method of Reed and Rilling with some modifications (20). For the kinetic analysis, 35 nM purified recombinant protein was incubated for 3 min in 100 μl of buffer containing 50 mM Tris, pH 7.7, 2 mM $MgCl_2$, 1 mM TCEP, and 5 μg/ml BSA. The concentrations of FPP and IPP ($^{14}C$-IPP, 400 kBq/μmol) were typically 0.05–20 μM. The remainder of the assay was completed as previously described in Ref. 8. For inhibition experiments, 10 μl of 10× N-BP was added to the enzyme in a total volume of 80 μl. After a 10-min preincubation (to allow for any slow binding inhibition), 20 μl of a substrate mixture containing FPP and IPP ($^{14}C$-IPP, 400 kBq/μmol) was added to start the reaction and giving a 10 μM final concentration for each substrate. Assays were carried out at 37 °C and subsequently terminated, extracted, and analyzed, as before (3). Preincubation of enzyme and inhibitor experiments showed tight binding characteristics, therefore data were evaluated as detailed previously (3). Reaction products were analyzed using thin layer chromatography (8). Silica Gel 60 TLC plates (Merck) spotted with reaction mixture were developed with propan-2-ol, ammonia, and water in a ratio of 9:3:1. Samples were identified by comparison with known standards and were visualized by staining with iodine vapor.

*Crystallization, Data Collection, Structure Solution, and Refinement*—PvGGPPS was crystallized in its apo form by mixing 1.5 μl of protein (at 16.5 mg/ml concentration in a buffer of 10 mM HEPES, pH 7.5, 500 mM NaCl) with 1.5 μl of reservoir solution consisting of 22% PEG 3350, 200 mM $Li_2SO_4$, 100 mM Tris, pH 8.5, in a hanging drop vapor diffusion setup with >350 μl of reservoir solution at 18 °C in VDXm plates (Hampton Research). For ZOL-added crystals, 1.5 μl of protein at 11.2 mg/ml containing an additional 10 mM ZOL, 10 mM IPP, and 10 mM $MgCl_2$ was mixed with 1.5 μl of reservoir solution (20% PEG 3350, 200 mM $Li_2SO_4$, 100 mM Tris, 8.5 at 18 °C) and incubated in hanging drops over 350 μl of reservoir solution. For GGPP-added crystals, 1.5 μl of protein (at 12.1 mg/ml in 10 mM HEPES, pH 7.5, 500 mM NaCl containing 1 mM GGPP and 2 mM $MgCl_2$) was mixed with 1.5 μl of reservoir solution consisting of 25% PEG 3350, 200 mM $(NH_4)_2SO_4$, 100 mM Tris, pH 8.5, and incubated in hanging drops over 350 μl of reservoir solution at 18 °C. In each case crystals appeared overnight. Crystals were flash cooled in $N_2$ (l). Data for apo and GGPP-bound crystals were collected on a Rigaku FR-E Superbright generator equipped with a Rigaku HTC image plate detector. The data for ZOL-incubated crystals were collected at the Cornell High Energy Synchrotron Source (CHESS), beam F1. Complete datasets were collected using 0.5° oscillations, and a total of 180° were collected. Native crystals diffracted to a maximum of 2.1 Å. The GGPP and ZOL crystals both diffracted to 2.5 Å, respectively. The native structure solution was obtained by molecular replacement using the program PHASER and Protein Data Bank (PDB) ID code 1UBV (*Gallus gallus* FPPS) as a model. Both ligand structures were subsequently solved using the original native PDB model as reference in PHASER. Initial maps from the molecular replacement for both sets showed obvious density for the ligands. All datasets and models were refined using REFMAC5 and the CCP4 package of programs. A test set consisting of 2% of the reflections was set aside for native data and 5% was set aside for both sets of ligand data. The final models have good geometry and no outliers in the Ramachandran analysis.

[3] Residue numbering for PvGGPPS is based on the sequence of PVX_092040 in PlasmoDB and differs from that found in the PDB structure files.

## RESULTS

### Plasmodium Prenylsynthases

Using the BLAST (21) utility served by the Web-based PlasmoDB database (17), the *P. falciparum* and *P. vivax* genes PF11_0295 and PVX_092040 were found to encode proteins 35–36% identical in sequence to human FPPS (HsFPPS) and 21–22% identical to human GGPPS (HsGGPPS). Similarly, they share a higher degree of sequence identity with FPPS than GGPPS from *S. cerevisiae*. Furthermore, the two *Plasmodium* orthologs are >70% identical to each other and approximately 30% identical to *Trypanosoma* and *Toxoplasma* FPPS as well as CpNPPPS, but less similar in sequence to GGPPS from *E. histolytica*.

In supplemental Fig. S1, the alignment of sequences of FPPS and/or GGPPS from humans, yeas,t and above-mentioned protozoan parasites are depicted. There is an insert of residues found specifically in the parasite prenylsynthases, including the kinetoplastids and apicomplexans, which is particularly long in the *Toxoplasma* enzyme and highly conserved between the two *Plasmodium* enzymes. Three of the critical sequence motifs identified in previous work (3, 8, 22), namely the first aspartate-rich motif (FARM), the second aspartate-rich motif (SARM) and the FPPS CLD region are also highlighted in supplemental Fig. S1. Previous studies indicate that (23, 24) two specific residues forming the CLD and starting 5 positions upstream of FARM limit the product length of FPPS to C15. These residues are both bulky in a specific FPPS and both small in GGPPS from humans, yeast, and *Entamoeba*. On the other hand, the reportedly bifunctional *Toxoplasma* FPPS (16) features a relatively small residue in cysteine and a large one in phenylalanine. Interestingly, both *Plasmodium* enzymes also have a similarly mixed pair in this position. Also distinctive is the asparagine in the fifth position in the SARM within HsGGPPS and ScGGPPS, where aspartate is present in all the other enzymes.

Previous analysis of structures of FPPS and (3, 6) have shown that the aspartates in FARM and SARM directly or indirectly (via water molecules) coordinate $Mg^{2+}$ to interact with phosphate groups in substrates and inhibitors. In the *Plasmodium* enzymes as well as all FPPSs, an aspartate occupies the fifth position of SARM, where both human and yeast GGPPS feature asparagine.

### Protein Expression and Activity Assays

We successfully expressed the *P. vivax* enzyme using an *Escherichia coli*-based expression platform proven to be effective for a significant number of apicomplexan proteins (19) but with two residues deviant from the sequence of PVX_092040 as published in PlasmoDB and NCBI (accession XP_001615401): T113M, N206D. This discrepancy may be attributed to either cloning mutation or genome sequencing error but is not part of any functional motif.

The activity of the recombinant protein was assayed using four potential allylic substrates, DMAPP, GPP, FPP, and GGPP. As indicated in Table 1 and Fig. 1, the enzyme catalyzed the conversion of all but GGPP. Among the productive substrates, the highest $k_{cat}$ value of 0.8 $s^{-1}$ was obtained for FPP, with $k_{cat}$ = ~0.5 $s^{-1}$ for DMAPP and GPP (Table 1). These rate constants are comparable with the values of 0.42 and 0.204 $s^{-1}$ obtained, respectively, for HsFPPS (3) and HsGGPPS (8). All three productive substrates had $K_m$ values in the low micromolar range (from 1.9 to 7.3 $\mu$M), as did IPP (8.4 $\mu$M), as found also for human (8) and yeast GGPPS (7). Judging $k_{cat}/K_m$ ratios in Table 1, the efficiency of the *Plasmodium* enzyme is lowest with FPP as the substrate (however, the differences vis-à-vis DMAPP and IPP are not significant) and roughly in the same range as that of human GGPPS (8). Most significantly, TLC analysis (Fig. 1) revealed GGPP to be the final product for each of the three allylic substrates. Based on this, we propose that, at least under the conditions tested, the *Plasmodium* enzyme is a GGPPS (traces of intermediate products were present due to premature stoppage of the reaction as also in product analysis of human FPPS and GGPPS assays) (3, 8). Such a finding is intriguing given that this is the only *Plasmodium* enzyme homologous to both HsFPPS and HsGGPPS.

**TABLE 1**

**Kinetic parameters of PvGGPPS**

Average values ± S.D. were obtained from multiple repetitions ($n > 5$) of the $^{14}C$ radioactivity assay described in Ref. 20.

| Substrate | Apparent $K_m$ | $V_{max}$ | $k_{cat}$ | $k_{cat}/K_m$ |
|---|---|---|---|---|
| | $\mu$M | *nmol/min per nmol* | $s^{-1}$ | $\mu M^{-1} s^{-1}$ |
| IPP | 8.4 ± 1.6 | | | |
| DMAPP | 3.2 ± 1.7 | 32.1 ± 1.7 | 0.5 | 0.2 |
| GPP | 1.9 ± 0.2 | 29.1 ± 1.0 | 0.5 | 0.3 |
| FPP | 7.3 ± 0.7 | 47.5 ± 1.6 | 0.8 | 0.1 |
| GGPP | | | | |

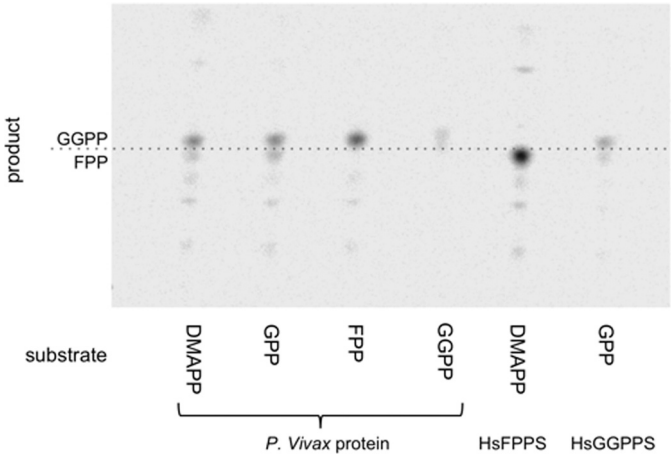


FIGURE 1. **Thin layer chromatography of products of *P. vivax* enzyme, human FPPS and GGPPS.** The *first four lanes* on the *left* show $^{14}C$ incorporation by products of the *P. vivax* enzyme from using GPP, DMAPP, FPP, and GGPP as substrates. The *last two lanes* on the *right* show $^{14}C$ incorporation by products of HsFPPS and HsGGPPS, included in the experiment as a control. Comparison with *HsGGPPS lanes* shows clearly that the *Plasmodium* enzyme produced GGPP with DMAPP, GPP, or FPP as allylic substrate. No product is seen in the *fourth lane*, representing the use of GGPP as the substrate, indicating that the product size is limited to C20. Both the human and *Plasmodium* proteins produced a trace amount of FPP when GPP was the substrate, as did the *Plasmodium* protein using DMAPP, all due to premature stoppage of the reaction.

### PvGGPPS Is Potently Inhibited by N-BPs

It has been previously reported that the PvGGPPS could be inhibited at submicromolar concentrations by bisphospho-

nates with and without nitrogen (18) (although the enzyme was assumed to be a FPPS in the study). The effectiveness of N-BPs is particularly interesting because these compounds have been found to be potent against FPPSs in general but ineffective on HsGGPPS (6). Accordingly, we chose three representative N-BPs, namely RIS, ZOL, and IBAN, to test against PvGGPPS under the same conditions as they were tested against HsFPPS (3), HsGGPPS (8), and CpNPPPS (12). Our experiments showed that all three compounds were more effective inhibitors by an order of magnitude than reported previously (18), with $IC_{50}$ values of 47.5 nM for RIS, 43.3 nM for ZOL, and 61.9 nM for IBAN and $K_i$ values also in the low nanomolar range (Table 2).

To the best of our knowledge, PvGGPPS is the only GGPPS studied to date that can be potently inhibited by N-BPs. We turned to structural biology to study this distinctive prenyl-synthase further and determine the mechanism of inhibition by N-BPs.

**TABLE 2**

**Inhibition of PvGGPPS by representative N-BPs ($n > 5$)**

Average values ± S.D. were obtained from multiple repetitions ($n > 5$) of the $^{14}C$ radioactivity assay described in Ref. 20.

| N-BP | $IC_{50}$ | $K_i^{app}$ | $K_i$ |
|---|---|---|---|
| | nM | nM | nM |
| RIS | 47.5 ± 4.4 | 29.7 ± 4.0 | 12.4 ± 1.7 |
| ZOL | 43.3 ± 3.3 | 25.8 ± 2.9 | 10.7 ± 1.2 |
| IBAN | 61.9 ± 4.1 | 38.3 ± 4.5 | 16.0 ± 1.9 |

### *Crystal Structures of PvGGPPS in Apo- and Ligand-bound Forms*

Structures of unliganded PvGGPPS (PDB ID code 3MAV; 2.1 Å; Fig. 2*A*), PvGGPPS/GGPP (PDB ID code 3PH7; 2.5 Å; Fig. 2*B*), and PvGGPPS/ZOL/IPP (PDB ID code 3LDW; 2.5 Å; Fig. 2*C*) were determined by means of x-ray crystallography, with the crystal parameters as well as processing and refinement data summarized in Table 3. Similar to FPPS structures but in contrast to the hexameric HsGGPPS (8), this protein is a homodimer of α-helices connected by loops of varying lengths (based on results of size exclusion chromatography; data not shown). In the crystals for all three structures, two dimers are in the asymmetric unit. In each subunit, the *N*-terminal two-helix hairpin (Fig. 2*A*) is curiously reminiscent of the FPPS fold (3, 25, 26) but distinct from both the single helix in the human GGPPS subunit (8) and the collinear pair of helices in ScGGPPS (7). The remaining helices of the PvGGPPS subunit, specifically α3–α14, form a cage-like arrangement common to both FPPS and other GGPPS to enclose a bicameral active site for housing the homoallylic and allylic substrates, as well as the eventual product. At the ends of helices α4 and α9, respectively, are the FARM and SARM, which

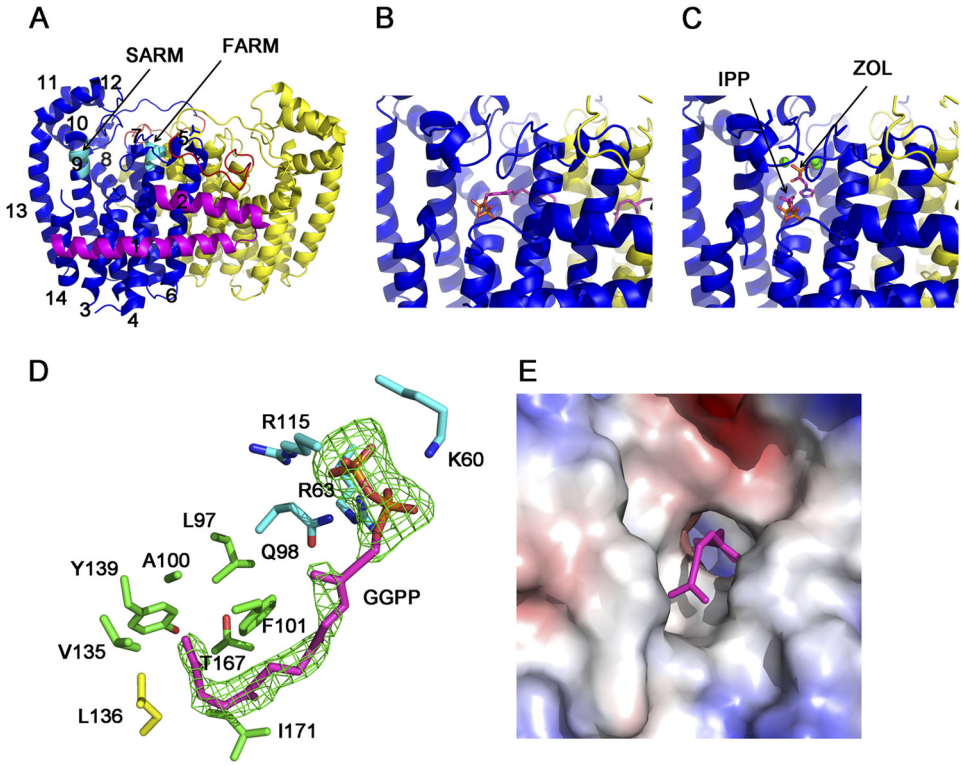


FIGURE 2. **PvGGPPS structures (all structures herein were rendered using PyMOL from Delano Scientific, Palo Alto, CA.** *A*, PvGGPPS apo-dimer (PDB ID code3MAV). The helices of the *blue* subunit are *numbered*. The N-terminal helical hairpin, consisting of α1 and α2, is *highlighted* in *magenta*. The FARM and SARM motifs are in *cyan*. The parasite-specific inserts are in *red*. *B*, active site of PvGGPPS occupied by product GGPP (PDB ID code 3PH7). *C*, active site of PvGGPPS occupied by IPP, ZOL, and magnesium ions (PDB ID code 3LDW). *D*, PvGGPPS active site. Close-up view shows the side chains around the two ends of GGPP: the key residues (carbon backbone in *cyan*) within hydrogen bonding distance of the pyrophosphate end and those forming a hydrophobic cavity (carbon backbone in *green* except for *yellow* $Leu^{136}$ from the other subunit) anchoring the aliphatic end. An $F_o - F_c$ omit map contoured at 2σ shows the electron density (in *green*) resulting from refinement of the complex without GGPP. A stereo figure of this active site is shown in supplemental Fig. S2. *E*, display of the electrostatic surface of a single subunit on the dimer interface side shows that, without the dimeric partner, the active site is wide open and may allow escape of the allylic substrate or intermediate product.

**TABLE 3**
**Data collection, phasing, and refinement statistics**

| Data collection | PvGGPPS-apo | PvGGPPS+ ZOL+ IPP | PvGGPPS+ GGPP |
|---|---|---|---|
| Space group | P21 | P212121 | P212121 |
| **Cell dimensions** | | | |
| *a* (Å) | 84.00 | 111.27 | 107.10 |
| *b* (Å) | 116.46 | 109.70 | 108.99 |
| *c* (Å) | 92.43 | 139.53 | 141.35 |
| $\alpha^\circ$ | 90.00 | 90.00 | 90.00 |
| $\beta^\circ$ | 116.01 | 90.00 | 90.00 |
| $\gamma^\circ$ | 90.00 | 90.00 | 90.00 |
| Wavelength | 1.5418 | 0.9179 | 1.5418 |
| Resolution | 50-2.1 | 25-2.5 | 50-2.5 |
| Measured reflections | 438,085 | 658,734 | 422,691 |
| Unique reflections | 92,263 | 60,963 | 57,809 |
| $R_{sym}$ | 0.054 (0.564) | 0.115 (0.657) | 0.051 (0.759) |
| $I/\sigma(I)$ | 35.4 (2.52) | 13.03 (2.03) | 39.83 (2.78) |
| Completeness (%) | 99.1 (96.6) | 100 (100) | 100 (100) |
| Redundancy | 4.7 (4.4) | 7.3 (7.2) | 7.3 (7.3) |
| PDB ID code | 3MAV | 3LDW | 3PH7 |
| **Refinement** | | | |
| Resolution | 20.99-2.1 | 25-2.5 | 40-2.5 |
| No. of reflections | 92,136 | 60,724 | 57,715 |
| Test set | 1,850 | 3,026 | 2,901 |
| $R_{work}/R_{free}$ | 0.229/0.262 | 0.243/0.285 | 0.237/0.273 |
| No. of atoms | 11,037 | 12,338 | 10,876 |
| Mean *B* factor | 46.29 | 34.21 | 68.77 |
| Ramachandran favored | 98 | 98.42 | 97.45 |
| Ramachandran disallowed | 0 | 0 | 0 |
| Root mean square deviations | | | |
| Bond lengths (Å) | 0.011 | 0.01 | 0.01 |
| Bond angles (°) | 0.92 | 1.33 | 1.07 |

contribute to binding of the allylic and homoallylic substrate in all prenylsynthases, *e.g.* Refs. 3, 7, 8, 12, 25, 26.

*Enzyme-Product Complex*—In the enzyme-product complex, GGPP is positioned with its pyrophosphate moiety in the homoallylic IPP chamber, forming hydrogen bonds with $Lys^{60}$, $Arg^{63}$, $Gln^{98}$, and $Arg^{115}$ (Fig. 2*D*). Overall, this highly hydrophilic region, where IPP is anchored before the condensation reaction, is conserved among FPPSs and GGPPSs. The middle portion of the aliphatic chain of GGPP is held in a channel within each subunit of PvGGPPS that is hydrophobic on the bottom and hydrophilic at the top. Interestingly, the CLD pair of phenylalanines in HsFPPS is aligned with $Ala^{100}$ and $Phe^{101}$ in PvGGPPS, where they form the wall of a hydrophobic cavity along with $Leu^{97}$, $Val^{135}$, $Tyr^{139}$, $Thr^{167}$, and $Ile^{171}$ (Fig. 2*D*). In the same figure, we can see that helix 6 from the dimer partner, specifically $Leu^{136}$, is complicit in closing this cavity. Without the presence of partner protein, as illustrated in the surface rendering of a single molecule of PvGGPPS in Fig. 2*E*, the hydrophobic end of the active site is wide open. This is distinctive from the yeast GGPPS structure (PDB ID code 2E8V), where each subunit provides complete self-containment of the GGPP pocket (7).

*Enzyme-Inhibitor Complex*—In the complex with ZOL and IPP (3LDW), the drug molecule interacts with the enzyme similarly to how N-BPs have been observed to bind FPPSs. First, the inhibitor is ensconced between the FARM- and SARM-containing helices via 3 $Mg^{2+}$ atoms that interact specifically with the bisphosphonate moiety in a fashion similar to that found in the human FPPS·ZOL·IPP complex (3, 26). Furthermore, the nitrogen atom in the drug molecule heterocycle forms hydrogen bonds with the carbonyl oxygen on $Lys^{222}$ and the $O^\gamma$ on $Thr^{223}$ (Fig. 3*A*). This N-Lys-Thr complex has also been previously described for HsFPPS (3, 26) and CpNPPPS (12) and is specifically responsible for the potent inhibition of both enzymes by N-BPs. More generally, the Lys-Thr pair is directly upstream of the kink on helix 8 and is conserved in all FPPSs as well as GGPPSs; however, variation between the two classes of prenylsynthases appears 4 positions downstream. Here, human and yeast GGPPSs feature a leucine and a phenylalanine ($Leu^{173}$ and $Phe^{174}$), creating a hydrophobic environment and counteracting to some degree the hydrogen bonding between nitrogen and the Lys-Thr pair (Fig. 3*B*). In contrast, as shown in Fig. 3*A*, both PvGGPPS and HsFPPS (and other FPPSs) feature a tyrosine ($Tyr^{226}$) and a serine ($Ser^{227}$) instead to create a comparatively polar environment. Although this effect distinguishes FPPSs and PvGGPPS from human and yeast GGPPSs, it does not fully explain the dramatically different levels of inhibition of these enzymes by N-BPs.

In the apo structure, the C-terminal tail, specifically the last four residues ($^{372}$FTGV$^{375}$), is flexible, as is the loop following SARM and connecting helices 9 and 10 (with the segment $^{272}$FGDSKKTGKVG$^{282}$ disordered). This leaves the "front" end of the active site wide open. In the ternary complex with ZOL and IPP, both regions are stabilized by ligand binding, resulting in a fully closed enzyme (Fig. 3*C*) and making the drug inaccessible to competition from the allylic substrate. A similar stabilization effect has been observed in HsFPPS (3, 26) where, however, the C-terminal tail is the primary segment blocking the active site once stabilized by the binding of IPP.

## DISCUSSION

Both humans and yeast have distinctive enzymes to produce FPP and GGPP, whereas our study shows the single *Plasmodium* homolog to be a GGPP synthase. Three types of GGPPSs have been described in the literature (16). Based on our results, *Plasmodium* GGPPS deviates from all of them while sharing a few features with FPPS, namely (i) higher shared sequence identity with FPPSs than with GGPPSs; (ii) a similar fold, including a N-terminal hairpin seen previously only in FPPS structures; (iii) conservation of one bulky phenylalanine in the FPPS-CLD position typically featuring small residues in GGPPSs; (iv) aspartate in the last position of SARM rather than asparagine; (v) potent inhibition by N-BPs. To the best of our knowledge, no other GGPPS has been found to be inhibited by ZOL or RIS at the same level of potency.

As indicated in Table 1, the *Plasmodium* enzyme can use any one of DMAPP, GPP, and FPP readily as an allylic substrate; however, with this enzyme established by our results as a GGPPS, there is not another prenyl synthase available as a FPPS candidate in the *Plasmodium* genomes, based on sequence homology. Given that a methylerythritol phosphate-based *Plasmodium* isoprenoid biosynthetic pathway producing IPP has been firmly established (27), it is very likely PvGGPPS synthesizes GGPP *in vivo* with DMAPP and IPP as starting materials. On the other hand, previous studies have demonstrated the presence of active *Plasmodium* farnesyl-

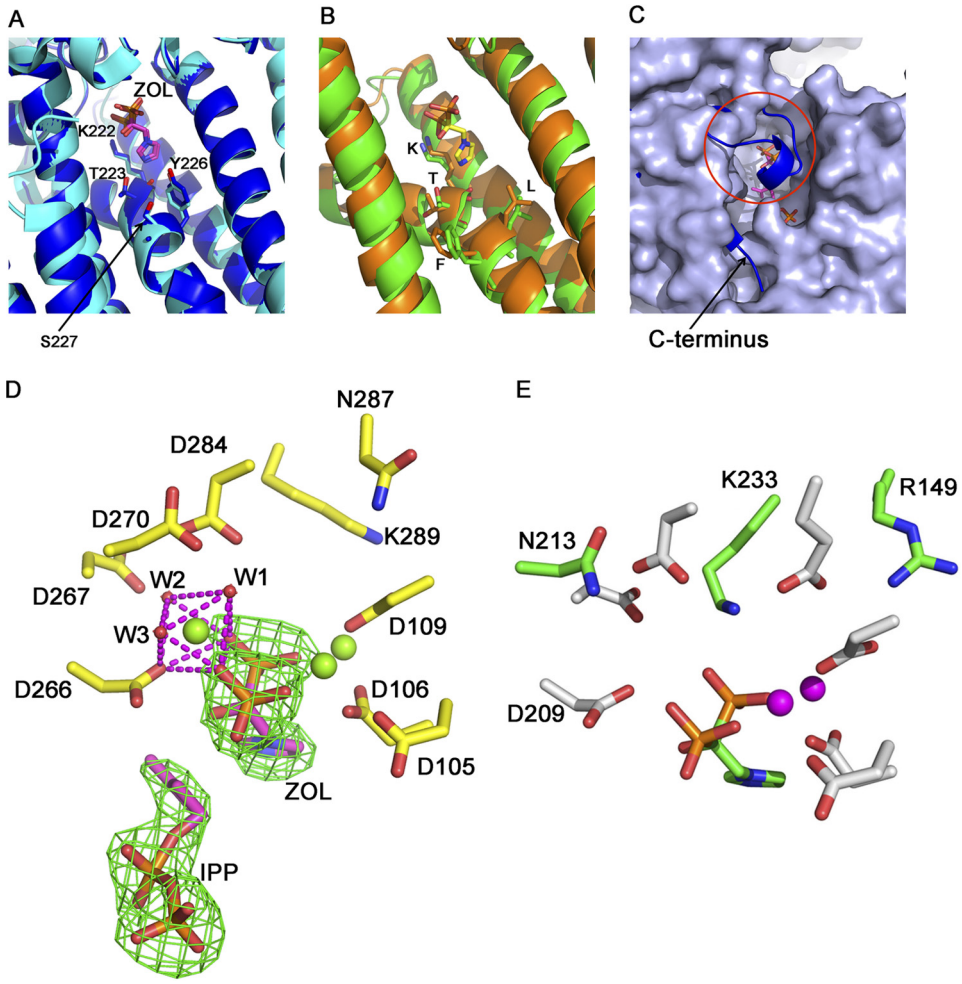


FIGURE 3. **ZOL binding.** Both FPPSs and GGPPSs contain a duo of lysine and threonine just upstream of the kink on helix 8 capable of forming a strong bifurcated hydrogen bond with a heterocyclic ZOL (and similar N-BPs). In addition, these enzymes typically interact with the pyrophosphate moiety via $Mg^{2+}$ and water molecules. *A*, in PvGGPPS (*blue*) and HsFPPS (*cyan*), as well as other FPPSs studied to date, there are also two residues downstream of the KT pair, namely tyrosine and serine, which form a polar region in place. Residues labeled are all from PvGGPPS. *B*, in most GGPPSs, including the human (*orange*) and yeast (*green*) enzymes, the N-Lys-Thr hydrogen-bonding complex is also conserved. In the vicinity of this interaction, there is a hydrophobic region formed by a Leu-Phe pair in place of the polar pair found in FPPS. The labeled residues are not numbered because they are the same in both human and yeast structures. *C*, surface rendering of apo-PvGGPPS superposed on schematic rendering (*blue*) of PvGGPPS with IPP and ZOL bound is shown. Both the C terminus and a loop connecting helices 9 and 10 (highlighted by a *red circle*) are stabilized by binding IPP. In particular, the stabilized loop blocks access to the active site and prevents competition with the drug molecule by the allylic substrate. *D*, PvGGPPS active site (3LDW) is shown. Three $Mg^{2+}$ help bridge the binding of ZOL to FARM and SARM. On the SARM side, the third $Mg^{2+}$ is coordinated by the phosphates on ZOL, water molecules W1, W2, and W3 as well as $Asp^{266}$ in a fashion similar to that seen in FPPS (3). The positions of ZOL and IPP are verified by their $F_o - F_c$ omit electron density maps contoured at $3\sigma$. A stereo figure of this active site is shown in supplemental Fig. S3. *E*, in the ScGGPPS/ZOL structure, there are only two $Mg^{2+}$ present, without a third metal ion to bridge SARM and ZOL. This may result from a change in the polar environment by the presence of the side chain of $Lys^{233}$ (*green*), which is forced into this area in human and yeast GGPPS by $Arg^{149}$ (*green*). Residue numbering is based on the scheme in Ref. 6. The substitution of asparagine (*N213* in *green*) for aspartate in the last position of SARM, also found in human GGPPS, may be a factor as well.

transferase and geranylgeranyltransferase in the ring, trophozoite, and schizont stages (28, 29), suggesting ability to utilize both FPP and GGPP in these malaria pathogens. Significantly, in the same study, it has also been found that radiolabeled farnesol is elongated by *Plasmodium* parasites into geranylgeraniol before being used for protein prenylation (28), clearly supporting the presence of a GGPP synthase. On the other hand, PFT-I inhibitors have been found to be effective in inhibiting parasitic growth (28), which seems to suggest FPP to be essential. This invites questions about their source for this C15 product. At least three possibilities exist: (i) There is another *Plasmodium* enzyme producing FPP as a final product, one which is completely unique in its amino acid sequence so as to escape identification to date. (ii) FPP is imported from the human host. (iii) The *Plasmodium* enzyme in our study is in fact bifunctional *in vivo*, even though it produces only GGPP under the experimental conditions described herein. The last scenario is possible because FPP is a requisite intermediate product in the biosynthesis of GGPP and may be released under specific conditions by the enzyme without being turned into the final product via a currently unknown mechanism. Confirmation of this in future studies may be accompanied by elucidation of how the enzyme manipulates the substrates and products of three sequential steps of condensation.

Magnesium coordination is a ubiquitous mechanism of bisphosphonate binding in prenyl synthases and generally in binding of ligands with phosphate moieties, with the number

of magnesium atoms varying among enzymes. In Ref. 6, it was first noted that the yeast GGPPS structures display a maximum of two $Mg^{2+}$, whether the ligand is a substrate or inhibitor, in contrast to typical complement of three found in FPPSs. Interestingly, our structure PvGGPPS in complex with ZOL and IPP displays three $Mg^{2+}$ involved in mediating the electrostatic interaction between the inhibitor and the FARM/SARM motifs, with two metal ions on the side of FARM and the remaining one on the other side facing SARM (Fig. 3*D*). Each $Mg^{2+}$ is coordinated by 8 oxygen atoms contributed by the phosphate groups in the inhibitor, aspartates in the FARM and SARM, as well as water molecules. Specifically, the SARM-bridging $Mg^{2+}$ is coordinated by ZOL, $Asp^{266}$ (the first aspartate in the SARM), and 3 water molecules labeled W1, W2, and W3 in Fig. 3*D*. The W1 molecule forms hydrogen bonds with two aspartates, $Asp^{270}$ and $Asp^{284}$, with the former being the last aspartate in the SARM. In the yeast GGPPS structure with ZOL bound (PDB ID 2E91 and Fig. 3*E*), the two $Mg^{2+}$ are both on the FARM side of the drug molecule, with the SARM-bridging metal ion absent. This is the case in almost all human and yeast GGPPS structures with 2 $Mg^{2+}$/protein molecule. As noted above, both of these enzymes feature Asn as the last residue in their SARM, in contrast to Asp in FPPSs and PvGGPPS. At the time of writing this article, there are only two *Saccharomyces* GGPPS structures available in the PDB with three $Mg^{2+}$ bound. In both cases, the ligand is an alkyl-BP. Likely due in part to the presence of $Asn^{213}$, their SARM-bridging magnesium is coordinated differently, using 4 rather than 3 water molecules, with $Asp^{209}$ (the first residue in the SARM motif) not participating directly. Notwithstanding the alternative coordination of the third metal ion, these A-BPs have been reported to be much more potent than ZOL in inhibiting yeast GGPPS (30). This supports the notion that the number of $Mg^{2+}$ is an important factor in determining inhibitor potency.

Differences in the SARM motif may not be the only cause of deviation among prenylsynthases in the use of $Mg^{2+}$ to coordinate phosphate groups. In human and yeast GGPPS, $Arg^{149}$, which is not found in FPPSs or PvGGPPS, pushes $Lys^{233}$ into the SARM region, numbering based on the scheme used for the yeast structure in (6). Together, the combination of a basic lysine and carboxamide-containing $Asn^{213}$ in the yeast enzyme may change the solvent environment around the SARM region so as to prevent the coordination of a third $Mg^{2+}$ in the manner seen in FPPSs and PvGGPPS.

Because *Plasmodium* cultures have been found to be much less sensitive to N-BPs than the kinetoplasts, *Toxoplasma* or *Cryptosporidium* (4, 10), our finding that *Plasmodium* GGPPS can be biochemically inhibited much more potently than previously believed is significant. This suggests the possibility that N-BPs may remain viable antimalarial candidates, if cell permeability problems described in the past (18) can be overcome with a next generation of compounds or transport enhancement. Furthermore, with an understanding of why N-BPs fail to affect HsGGPPS, it may be possible to modify existing drugs to permit a full complement of metal coordination and therefore improve the inhibition potency.

Finally, we believe that the structural and functional interpretations presented herein about the PvGGPPS enzyme are applicable to the *P. falciparum* ortholog. This is because the two proteins share 70% sequence identity, with nearly identical residues in key function-defining regions (supplemental Fig. S1).

*Acknowledgments—We thank Helen Ren and Carmen Khuu for large scale expression of the PvGGPPS protein. The BL21(DE3)R3-pRARE2 strain of E. coli used in expressing the proteins came from Opher Gileadi of the Structural Genomics Consortium (SGC) at the University of Oxford. The cDNA for PvGGPPS was a generous gift from Prof. Liwang Cui of Pennsylvania State University.*

## REFERENCES

1. Dunford, J. E., Kwaasi, A. A., Rogers, M. J., Barnett, B. L., Ebetino, F. H., Russell, R. G., Oppermann, U., and Kavanagh, K. L. (2008) *J. Med. Chem.* **51,** 2187–2195
2. Dunford, J. E., Thompson, K., Coxon, F. P., Luckman, S. P., Hahn, F. M., Poulter, C. D., Ebetino, F. H., and Rogers, M. J. (2001) *J. Pharmacol. Exp. Ther.* **296,** 235–242
3. Kavanagh, K. L., Guo, K., Dunford, J. E., Wu, X., Knapp, S., Ebetino, F. H., Rogers, M. J., Russell, R. G., and Oppermann, U. (2006) *Proc. Natl. Acad. Sci. U.S.A.* **103,** 7829–7834
4. Ghosh, S., Chan, J. M., Lea, C. R., Meints, G. A., Lewis, J. C., Tovian, Z. S., Flessner, R. M., Loftus, T. C., Bruchhaus, I., Kendrick, H., Croft, S. L., Kemp, R. G., Kobayashi, S., Nozaki, T., and Oldfield, E. (2004) *J. Med. Chem.* **47,** 175–187
5. Szabo, C. M., Matsumura, Y., Fukura, S., Martin, M. B., Sanders, J. M., Sengupta, S., Cieslak, J. A., Loftus, T. C., Lea, C. R., Lee, H. J., Koohang, A., Coates, R. M., Sagami, H., and Oldfield, E. (2002) *J. Med. Chem.* **45,** 2185–2196
6. Guo, R. T., Cao, R., Liang, P. H., Ko, T. P., Chang, T. H., Hudock, M. P., Jeng, W. Y., Chen, C. K., Zhang, Y., Song, Y., Kuo, C. J., Yin, F., Oldfield, E., and Wang, A. H. (2007) *Proc. Natl. Acad. Sci. U.S.A.* **104,** 10022–10027
7. Chang, T. H., Guo, R. T., Ko, T. P., Wang, A. H., and Liang, P. H. (2006) *J. Biol. Chem.* **281,** 14991–15000
8. Kavanagh, K. L., Dunford, J. E., Bunkoczi, G., Russell, R. G., and Oppermann, U. (2006) *J. Biol. Chem.* **281,** 22004–22012
9. Montalvetti, A., Bailey, B. N., Martin, M. B., Severin, G. W., Oldfield, E., and Docampo, R. (2001) *J. Biol. Chem.* **276,** 33930–33937
10. Martin, M. B., Grimley, J. S., Lewis, J. C., Heath, H. T., 3rd, Bailey, B. N., Kendrick, H., Yardley, V., Caldera, A., Lira, R., Urbina, J. A., Moreno, S. N., Docampo, R., Croft, S. L., and Oldfield, E. (2001) *J. Med. Chem.* **44,** 909–916
11. Gabelli, S. B., McLellan, J. S., Montalvetti, A., Oldfield, E., Docampo, R., and Amzel, L. M. (2006) *Proteins* **62,** 80–88
12. Artz, J. D., Dunford, J. E., Arrowood, M. J., Dong, A., Chruszcz, M., Kavanagh, K. L., Minor, W., Russell, R. G., Ebetino, F. H., Oppermann, U., and Hui, R. (2008) *Chem. Biol.* **15,** 1296–1306
13. Ling, Y., Sahota, G., Odeh, S., Chan, J. M., Araujo, F. G., Moreno, S. N., and Oldfield, E. (2005) *J. Med. Chem.* **48,** 3130–3140
14. Moreno, B., Bailey, B. N., Luo, S., Martin, M. B., Kuhlenschmidt, M., Moreno, S. N., Docampo, R., and Oldfield, E. (2001) *Biochem. Biophys. Res. Commun.* **284,** 632–637
15. Singh, A. P., Zhang, Y., No, J. H., Docampo, R., Nussenzweig, V., and Oldfield, E. (2010) *Antimicrob. Agents Chemother.* **54,** 2987–2993
16. Ling, Y., Li, Z. H., Miranda, K., Oldfield, E., and Moreno, S. N. (2007) *J. Biol. Chem.* **282,** 30804–30816
17. Bahl, A., Brunk, B., Crabtree, J., Fraunholz, M. J., Gajria, B., Grant, G. R., Ginsburg, H., Gupta, D., Kissinger, J. C., Labo, P., Li, L., Mailman, M. D., Milgram, A. J., Pearson, D. S., Roos, D. S., Schug, J., Stoeckert, C. J., Jr., and Whetzel, P. (2003) *Nucleic Acids Res.* **31,** 212–215
18. Mukkamala, D., No, J. H., Cass, L. M., Chang, T. K., and Oldfield, E.

(2008) *J. Med. Chem.* **51,** 7827–7833
19. Vedadi, M., Lew, J., Artz, J., Amani, M., Zhao, Y., Dong, A., Wasney, G. A., Gao, M., Hills, T., Brokx, S., Qiu, W., Sharma, S., Diassiti, A., Alam, Z., Melone, M., Mulichak, A., Wernimont, A., Bray, J., Loppnau, P., Plotnikova, O., Newberry, K., Sundararajan, E., Houston, S., Walker, J., Tempel, W., Bochkarev, A., Kozieradzki, I., Edwards, A., Arrowsmith, C., Roos, D., Kain, K., and Hui, R. (2007) *Mol. Biochem. Parasitol.* **151,** 100–110
20. Reed, B. C., and Rilling, H. C. (1975) *Biochemistry* **14,** 50–54
21. Altschul, S. F., Gish, W., Miller, W., Myers, E. W., and Lipman, D. J. (1990) *J. Mol. Biol.* **215,** 403–410
22. Chen, A., Kroon, P. A., and Poulter, C. D. (1994) *Protein Sci.* **3,** 600–607
23. Ohnuma, S., Narita, K., Nakazawa, T., Ishida, C., Takeuchi, Y., Ohto, C., and Nishino, T. (1996) *J. Biol. Chem.* **271,** 30748–30754
24. Tarshis, L. C., Proteau, P. J., Kellogg, B. A., Sacchettini, J. C., and Poulter, C. D. (1996) *Proc. Natl. Acad. Sci. U.S.A.* **93,** 15018–15023
25. Tarshis, L. C., Yan, M., Poulter, C. D., and Sacchettini, J. C. (1994) *Biochemistry* **33,** 10871–10877
26. Rondeau, J. M., Bitsch, F., Bourgier, E., Geiser, M., Hemmig, R., Kroemer, M., Lehmann, S., Ramage, P., Rieffel, S., Strauss, A., Green, J. R., and Jahnke, W. (2006) *Chem. Med. Chem.* **1,** 267–273
27. Clastre, M., Goubard, A., Prel, A., Mincheva, Z., Viaud-Massuart, M. C., Bout, D., Rideau, M., Velge-Roussel, F., and Laurent, F. (2007) *Exp. Parasitol.* **116,** 375–384
28. Chakrabarti, D., Da Silva, T., Barger, J., Paquette, S., Patel, H., Patterson, S., and Allen, C. M. (2002) *J. Biol. Chem.* **277,** 42066–42073
29. Chakrabarti, D., Azam, T., DelVecchio, C., Qiu, L., Park, Y. I., and Allen, C. M. (1998) *Mol. Biochem. Parasitol.* **94,** 175–184
30. Chen, K.-M., Hudock, M. P., Zhang, Y., Guo, R. T., Cao, R., No, J. H., Liang, P. H., Ko, T. P., Chang, T. H., Chang, S. C., Song, Y., Axelson, J., Kumar, A., Wang, A. H., and Oldfield, E. (2008) *J. Med. Chem.* **51,** 5594–5607